

# Pressure-induced volume-collapsed tetragonal phase of $\text{CaFe}_2\text{As}_2$ as seen via neutron scattering

A. Kreyssig<sup>1,2</sup>, M. A. Green<sup>3,4</sup>, Y. Lee<sup>1,2</sup>, G. D. Samolyuk<sup>1,2</sup>, P. Zajdel<sup>3,5</sup>, J. W. Lynn<sup>3</sup>,  
S. L. Bud'ko<sup>1,2</sup>, M. S. Torikachvili<sup>6</sup>, N. Ni<sup>1,2</sup>, S. Nandi<sup>1,2</sup>, J. Leão<sup>3</sup>, S. J. Poulton<sup>3,4</sup>,  
D. N. Argyriou<sup>7</sup>, B. N. Harmon<sup>1,2</sup>, R. J. McQueeney<sup>1,2</sup>, P. C. Canfield<sup>1,2</sup>, and A. I. Goldman<sup>1,2</sup>

<sup>1</sup>Ames Laboratory, US DOE; Ames, IA 50011; USA

<sup>2</sup>Department of Physics and Astronomy, Iowa State University; Ames, IA 50011; USA

<sup>3</sup>NIST Center for Neutron Research, National Institute of Standards and Technology; Gaithersburg, MD 20899; USA

<sup>4</sup>Department of Materials Science and Engineering,

University of Maryland; College Park, MD 20742; USA

<sup>5</sup>Department of Chemistry, University College of London; 20 Gordon Street; London, W1X 0AJ; UK

<sup>6</sup>Department of Physics, San Diego State University; San Diego, CA 92182; USA and

<sup>7</sup>Helmholtz-Zentrum Berlin für Materialien und Energie; Glienicker Str. 100; 14109 Berlin; Germany

Recent investigations of the superconducting iron-arsenide families have highlighted the role of pressure, be it chemical or mechanical, in fostering superconductivity. Here we report that  $\text{CaFe}_2\text{As}_2$  undergoes a pressure-induced transition to a non-magnetic, volume “collapsed” tetragonal phase, which becomes superconducting at lower temperature. Spin-polarized total-energy calculations on the collapsed structure reveal that the magnetic Fe moment itself collapses, consistent with the absence of magnetic order in neutron diffraction.

PACS numbers: 61.50.Ks, 61.05.fm, 71.15.Nc, 74.62.Fj; Paper accepted for publication in Phys. Rev. B

Two recently discovered[1, 2, 3, 4] series of high transition temperature (high- $T_c$ ) superconductors originate from the parent systems  $R\text{FeAsO}$  ( $R$  = rare earth) and  $A\text{Fe}_2\text{As}_2$  ( $A$  = alkaline earth metal), which are tetragonal at room temperature but undergo an orthorhombic distortion in the range 100-220 K that is associated with the onset of antiferromagnetic order[5, 6, 7, 8, 9, 10, 11]. Tuning the system via element substitution[2, 3, 4, 12, 13, 14] or oxygen deficiency[15, 16] suppresses the magnetic order and structural distortion in favor of superconductivity ( $T_c$ 's up to 55 K), with an overall behavior strikingly similar to the high- $T_c$  copper oxide family of superconductors.

The recent report[17] of pressure-induced superconductivity in the parent  $\text{CaFe}_2\text{As}_2$  compound opens an alternative path to superconductivity. Pressure suppresses the distinct resistivity signature of the high-temperature structural and magnetic phase transition from 170 K at ambient pressure[18] to 128 K at 0.35 GPa[17]. Superconductivity emerges with  $T_c$  up to 12 K for pressures between 0.23 GPa and 0.86 GPa[17]. The pressure-induced superconductivity in  $\text{CaFe}_2\text{As}_2$  was confirmed[19] and followed by observations of superconductivity for  $\text{BaFe}_2\text{As}_2$  and  $\text{SrFe}_2\text{As}_2$  at significantly higher pressures[20]. In  $\text{CaFe}_2\text{As}_2$ , a second high-temperature phase transition is observed above 0.55 GPa and 104 K by anomalies in the resistivity[17]. However, the nature of the phase at temperatures below this transition and its relation to the ambient-pressure tetragonal, orthorhombic and pressure-induced superconducting phases are as yet unknown.

Neutron scattering experiments on  $\text{CaFe}_2\text{As}_2$  were performed to elucidate these issues. Special attention

was paid to maintain experimental conditions closest to the reported macroscopic measurements and under well-defined hydrostatic pressure. Therefore, the experiments were performed on a polycrystalline sample prepared out of approximately 1.75 grams of single crystalline  $\text{CaFe}_2\text{As}_2$  material grown using the procedure described in references [18] and [21]. The temperature profile for preparing this material was slightly modified (heating to 1100°C and cooling over 50 hours to 600°C) to inhibit the formation of the reported[18] needle-shaped impurity phase. Temperature-dependent resistance measurements on these crystals reproduced the data presented in references [17] and [18]. The single crystals (300 pieces) were loaded with attempted random orientation into a He-gas pressure cell (maximum pressure 0.63 GPa) and measured on the BT1 high-resolution powder diffractometer at the NIST Center for Neutron Research. To reduce the effects of preferred orientation, the sample was oscillated over an angle of 36 deg during each measurement. For the temperature-dependent studies, the temperature was slowly changed with a maximum rate of 5 K/min while the pressure was adjusted and allowed to equilibrate between measurements.

Figure 1 shows neutron diffraction scans taken through the nuclear  $(0\ 0\ 2)$ ,  $(2\ 2\ 0)_T$ , and magnetic  $(1\ 2\ 1)_{\text{OR, magnetic}}$  diffraction peaks at selected temperatures and pressures. At 50 K and ambient pressure (A), the splitting of the  $(2\ 2\ 0)_T$  into the orthorhombic  $(4\ 0\ 0)_{\text{OR}}/(0\ 4\ 0)_{\text{OR}}$  peaks signals the transformation to the orthorhombic phase (Fig. 1(b)). This, together with the observation of the magnetic  $(1\ 2\ 1)_{\text{OR, magnetic}}$  peak (Fig. 1(c)), is consistent with previous x-ray and neutron diffraction measurements at ambient pressure[10, 18].

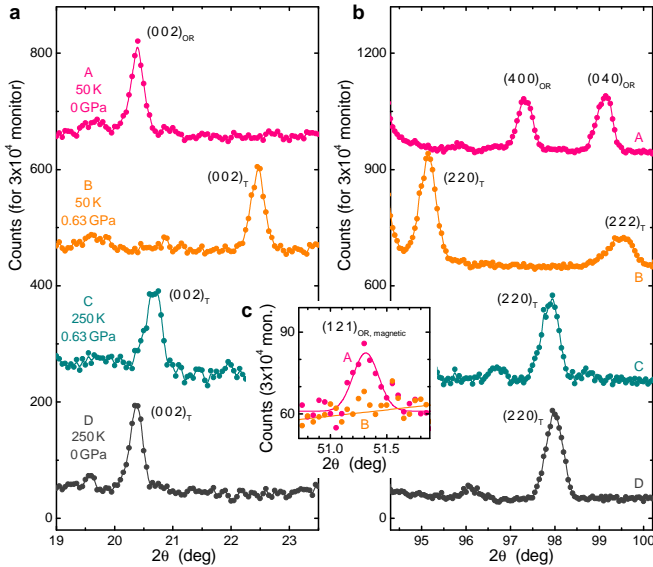


FIG. 1: (color online) Scans through (a-b) nuclear and (c) magnetic peaks in neutron diffraction pattern at selected temperatures and pressures. Note that the diffraction peaks change position dramatically due to the significant changes in the lattice parameters. In (c), the magnetic  $(1\ 2\ 1)_{\text{OR, magnetic}}$  diffraction peak for point A is clearly observed above the background taken at B. No new magnetic peaks for B and C were observed. Unlabelled peaks in the pattern arise from phases other than  $\text{CaFe}_2\text{As}_2$ , such as minor contamination from the Sn flux or  $\text{SiO}_2$  (silica wool or pieces of the silica ampule from the single crystal growth), or the pressure cell. The subscripts denote the crystal structure used for indexing (T = tetragonal; OR = orthorhombic). The offset between every data set is 200 Counts/ $3 \times 10^4$  monitor in (a) and 300 Counts/ $3 \times 10^4$  monitor in (b), respectively.

Upon increasing pressure at  $T = 50$  K, the structure remains orthorhombic and antiferromagnetic up to approximately 0.24 GPa.

Between 0.24 and 0.35 GPa, dramatic changes take place in the measured diffraction patterns. At pressures above 0.35 GPa (Fig. 1(c)), the magnetic peak is absent. No other magnetic peaks (e.g. corresponding to the AF1 magnetic phase proposed in reference [22]) are observed. The orthorhombic structure has transformed to a tetragonal phase, similar to the high-temperature ambient pressure structure, but with extraordinarily different lattice parameters. This is most evident from the strong shift in the positions of the  $(0\ 0\ 2)$  and  $(2\ 2\ 0)_{\text{T}}$  peaks at (B) in Figs. 1(a) and 1(b), respectively. The structure of this pressure-induced “collapsed” tetragonal phase is unchanged in the superconducting state determined by measurements at 4 K and under 0.48 GPa.

The central region (shown in yellow) of Figs. 2(b) and (c) shows the results of Rietveld refinements of the lattice parameters and volume for the “collapsed” tetragonal phase. The structure data (lattice parameters and atomic-position parameter  $z_{\text{As}}$  of As) were deter-

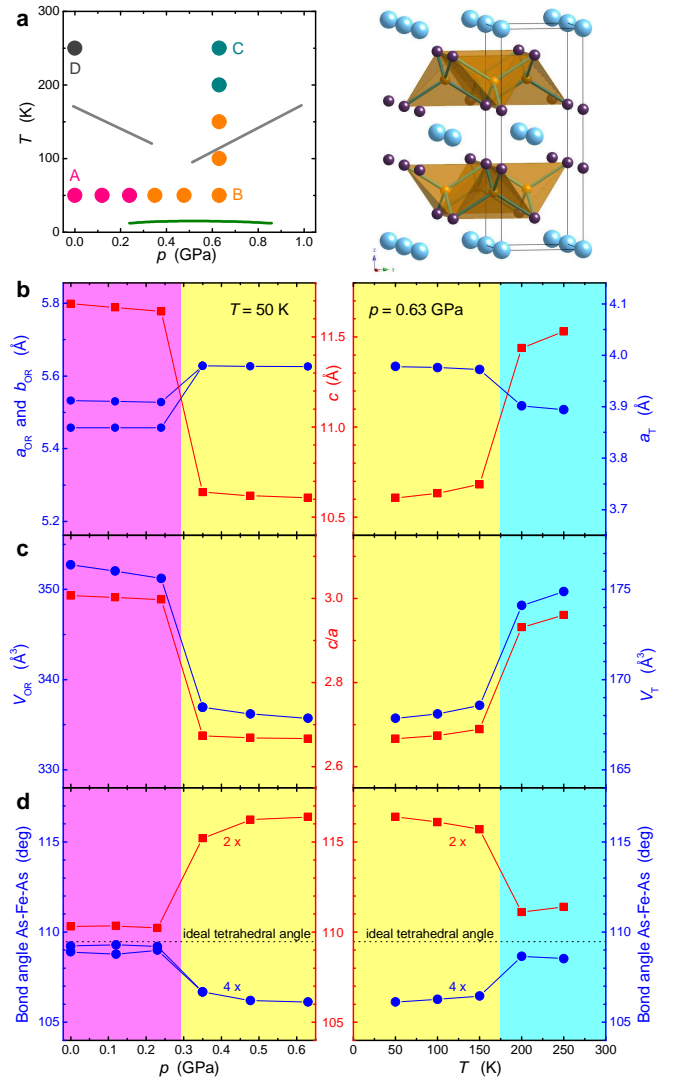


FIG. 2: (color online) Schematic phase diagram and pressure and temperature dependence of the lattice parameters, unit cell volume and As-Fe-As bond angles. (a) (left panel) Lines in the schematic  $p - T$  diagram denote the high-temperature and superconductivity phase lines determined in reference [17]. Points A-D label the pressures and temperatures for the diffraction data shown in Figure 1. (a) (right panel) The unit cell of the tetragonal phase of  $\text{CaFe}_2\text{As}_2$ . (b-d) Pressure dependence (left panels) at  $T = 50$  K and temperature dependence (right panels) at  $p = 0.63$  GPa (b) of the lattice parameters, (c) of the unit cell volume and  $c/a$  ratio, and (d) of the As-Fe-As bond angle.

mined by Rietveld refinements using the GSAS software package[23]. We find an astonishing 9.5% reduction in the  $c$ -lattice parameter with respect to the orthorhombic phase and a nearly 5% decrease in the unit cell volume. Even more striking is the reduction of the  $c/a$  ratio, a key parameter for bond geometries in the iron arsenides, by nearly 11%. As a consequence, the As-Fe-As bond angles change strongly as illustrated in Fig. 2(d).

With the pressure maintained at 0.63 GPa, the temper-

ature was raised in 50 K steps (right panels of Fig. 2). Between 150 and 200 K an isostructural transition between the low-temperature “collapsed” tetragonal phase and the high-temperature tetragonal structure is observed. Upon release of the pressure at 250 K, the curves labelled (D) in Fig. 1 show only small changes in the lattice parameters between 0.63 GPa and ambient pressure, providing a measure of the modest, but strongly anisotropic compressibility of the high-temperature phase.

We note that there is a difference of about 50 K between the temperature of the isostructural transition at 0.63 GPa measured here and that reported in transport measurements[17]. However, as pointed out in Ref. [17], the resistive anomalies are rather broad in applied pressure, and different criteria for the definition of transition temperatures can shift temperature assignments. In addition, the data in Ref. [17] were taken with decreasing temperature whereas here the temperature was step-wise increased. With these uncertainties understood, the tetragonal-to-“collapsed” tetragonal transition appears to be responsible for the loss of resistivity whose locus defines the high-temperature high-pressure phase line found in Ref. [17] and shown in Fig. 2(a).

In order to relate the volume change to relative changes in the unit cell dimensions, and to verify the stability of this phase, spin-polarized total-energy calculations were performed for volume changes of  $\Delta V/V = 0\%$  (for ambient pressure) and  $\Delta V/V = -5\%$  (for the “collapsed” phase). The local density approximation was employed, using the full potential linearized augmented plane wave method with the Perdew-Wang 1992 functional[24]. The precision of the total energy is 0.01 mRyd/cell, much smaller than the size of the symbols in Fig. 3.

From the blue (dark grey) curves in Fig. 3(a) we see that, for ambient pressure, the orthorhombic magnetic phase is lowest in energy, consistent with our ambient-pressure low-temperature measurement. The red (light grey) curves in Fig. 3(a) show that the tetragonal phase is lowest in total energy for the 5% volume reduction. The minimum energy of this “collapsed” tetragonal phase is found at  $c/a \sim 2.65$ , close to the experimental value of 2.67 (Fig. 2(c)).

The  $c/a$ -dependence of the spin-polarized total-energy calculations for the “collapsed” phase can be correlated with a loss of the Fe magnetic moment, as shown in Fig. 3(b). Both the spin-polarized and non-spin-polarized calculations yield the same total-energy minimum for the non-magnetic “collapsed” tetragonal phase at the same  $c/a$  ratio. The astonishing result of a quenched magnetic moment ground state is consistent with our experimental observation of the loss of magnetic order in the “collapsed” tetragonal phase. The band structure calculations also indicate that several bands cross the Fermi level at the pressure-induced transition.

The principal result of these neutron diffraction measurements is the discovery of a transition from the

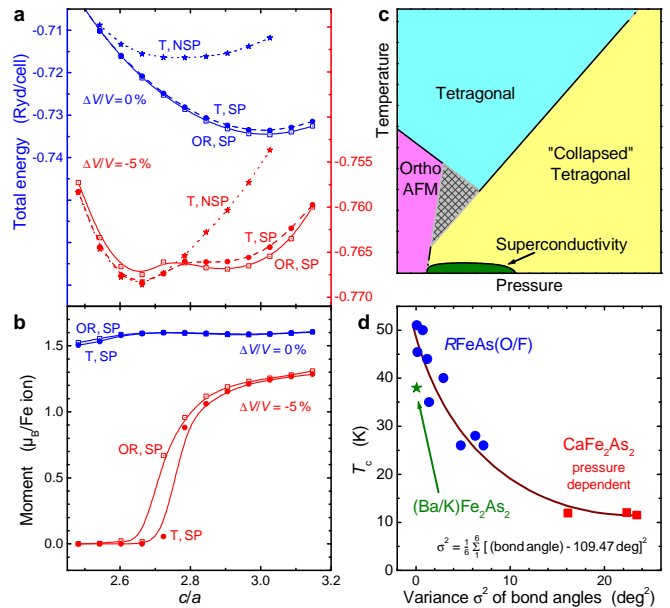


FIG. 3: (color online) Summary of the results of the neutron diffraction measurements and total-energy calculations. (a) Spin-polarized (SP) and non-spin-polarized (NSP) total-energy calculations for  $\Delta V/V = 0\%$  and  $\Delta V/V = -5\%$  for the tetragonal (T) and orthorhombic (OR) phases (Note the different energy scales). The tetragonal notation is used for the  $c/a$  ratio. (b) For the “collapsed” phase, the Fe moment is quenched at the minimum in total energy in the spin-polarized calculation. (c) Schematic  $p - T$  diagram based upon the diffraction and transport[17] measurements. Dashed lines represent estimates of the phase boundaries. The cross hatched area indicates a region where precise details of how these transition lines intersect still needs to be determined. (d) Correlation between the superconducting transition temperatures and the variance  $\sigma^2$  of the As-Fe-As bond angle. The data were obtained from Refs. [5] and [25, 26, 27, 28, 29] for the  $R\text{FeAs(O/F)}$  compounds and from Ref. [4] for  $(\text{Ba/K})\text{Fe}_2\text{As}_2$ , respectively. The data for  $\text{CaFe}_2\text{As}_2$  are derived from the present measurements.

magnetically ordered orthorhombic phase to a non-magnetically ordered “collapsed” tetragonal phase preceding the onset of superconductivity. Further, the second, higher pressure, transition noted in transport measurements[17] has been identified as an isostructural transition between the pressure-induced “collapsed” phase and the high-temperature tetragonal structure. The observed volume reduction can, for example, serve to increase the charge-carrier density. The schematic phase diagram in Fig. 3(c) summarizes our findings. Our results show that the pressure-induced superconductivity[17] in  $\text{CaFe}_2\text{As}_2$  emerges from the “collapsed” tetragonal phase rather than the magnetically ordered, orthorhombic phase or the high-temperature tetragonal phase.

Anomalous changes in the unit cell volume and lattice constants have also been noted in the  $R\text{FeAsO}$  system. In superconducting fluorine-free oxygen-deficient samples

of  $\text{NdFeAsO}_{1-\delta}$ , a surprising discontinuous decrease in the lattice parameters and unit cell volume ( $\Delta V/V = -1.8\%$ ) was found for  $\delta = 0.4$ , where a maximum in the superconducting volume fraction is observed[16]. Furthermore, a correlation between superconducting transition temperatures for  $R\text{FeAsO}_{1-\delta}$  and the unit cell dimensions is reported[15]. In light of our results, it appears that chemical substitution and the introduction of oxygen deficiency likely play a dual role in the iron arsenide superconductors by increasing the charge carrier density and changing the “chemical pressure”. It is not yet clear which has the greater impact upon superconductivity.

Given that the  $R\text{FeAsO}$  and  $\text{AFe}_2\text{As}_2$  families share a common structural element (FeAs layers) and similar prerequisites for superconductivity (e.g. suppression of magnetic order) it is useful to elucidate structural quantities that are shared and can be correlated with superconducting properties. Of particular interest is the comparison of the As-Fe-As bond angles[25] with the ideal tetrahedral value of 109.47 deg. For this special value all Fe atoms are coordinated in ideally formed tetrahedrons with identical high-symmetric Fe-As-Fe bonding geometries [highlighted in brown in the right panel of Fig. 2(a)]. This symmetry is broken for As-Fe-As bond angles deviating from this ideal angle yielding two or three different values in the tetragonal or orthorhombic structure, respectively.

The variance  $\sigma^2 = \frac{1}{6} \sum_1^6 [(\text{bond angle}) - 109.47 \text{ deg}]^2$  in deviation of the Fe-As-Fe bonding angles from the ideal value parameterizes the strength of this symmetry breaking.

In Figure 3(d) we plot the measured superconducting transition temperatures  $T_c$ , for those iron-arsenide compounds that are superconducting, as a function of this variance  $\sigma^2$  of the As-Fe-As bond angles. As  $\sigma^2$  increases, corresponding to greater deviations in the bond angle from the ideal tetrahedral angle,  $T_c$  decreases. The pressure-dependent properties of the “collapsed” tetragonal phase of  $\text{CaFe}_2\text{As}_2$  described above clearly continue this trend and allow generalizing our result to the family of FeAs based superconductors. The high value for  $\sigma^2$  in the “collapsed” tetragonal phase for  $\text{CaFe}_2\text{As}_2$  is consistent with the low  $T_c$  in comparison to other FeAs based superconductors. The observed correlation between  $T_c$  and  $\sigma^2$  points to the importance of the structure and the symmetry in the FeAs network for the superconducting state. Properties that are sensitive to the As-Fe-As bonding geometry and its symmetry, such as anisotropic magnetic or elastic couplings in the FeAs network, seem strongly involved in the superconducting pairing.

These results highlight intriguing questions that point to the potential complexity of the superconducting state in the iron arsenides. From the analysis of  $T_c$  as a function of the As-Fe-As bond angle variance, we have found that superconductivity in the “collapsed” tetragonal

phase fits well within the general trend observed for the doped iron arsenides, implying a common superconducting pairing mechanism. It has been suggested that spin fluctuations are responsible for the electron pairing in this class of superconductors[30]. The apparent loss of a static moment in the “collapsed” tetragonal phase may seem inconsistent with such a magnetic pairing mechanism for the pressure-induced superconductivity in  $\text{CaFe}_2\text{As}_2$ . However, the strong pair-breaking effect of local moments is eliminated and superconductivity mediated by paramagnons[31] remains a possibility.

The authors wish to acknowledge very useful discussions with Joerg Schmalian. Work at the Ames Laboratory was supported by the US Department of Energy - Basic Energy Sciences under Contract No. DE-AC02-07CH11358. M. S. Torikachvili acknowledges support by the National Science Foundation under DMR-0306165 and DMR-0805335.

#### APPENDIX A: DETAILS OF THE NEUTRON DIFFRACTION MEASUREMENTS AND THEIR ANALYSIS INCLUDING STRUCTURE DATA

The neutron diffraction measurements were performed on the high resolution powder diffractometer BT1 at the NIST Center for Neutron Research using a wavelength of 2.0782 Å selected by a Ge (3 1 1) monochromator. The collimation of the incident beam was set at 15’.

Special attention was paid to maintaining experimental conditions closest to the reported macroscopic measurements and to perform the study under well-defined hydrostatic pressure. The soft and ductile nature of the compound presents challenges for powder diffraction measurements since flux-grown single crystals tend to smear and shear when ground into a powder. The effects of grinding are clearly observed as broadened peaks in x-ray powder diffraction measurements, and the modification of physical properties associated with grinding have not yet been characterized. Therefore, as grown single crystals (~500-1000) were loaded into an Al-alloy He-gas pressure cell and cooled using a top-loading closed-cycle cryogenic refrigerator. The pressure cell was connected to a pressurizing intensifier through a high pressure capillary. Hydrostatic pressure was maintained throughout the measurements since the temperature was kept well above the melting curve for helium (for pressures up to 0.63 GPa). For the temperature dependence studies, the temperature was slowly changed with a maximum rate of 5 K/min while the pressure was adjusted and allowed to equilibrate between measurements.

To reduce the effects of preferred orientation, the sample was oscillated over an angle of 36 deg during each measurement. Nevertheless, a degree of preferred orientation remained but was adequately modelled in sub-

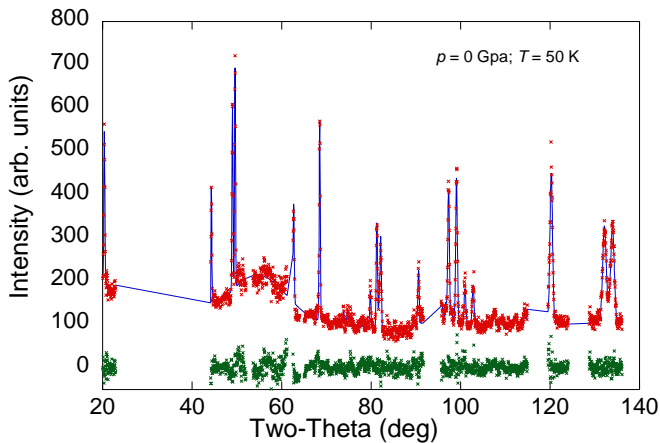


FIG. 4: (color online) Rietveld analysis of the neutron diffraction pattern at  $p = 0$  Gpa and  $T = 50$  K. Areas with strong contributions from the pressure cell are excluded.

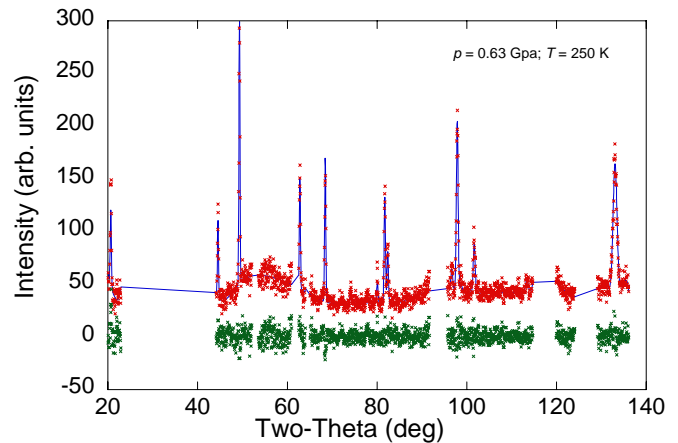


FIG. 6: (color online) Rietveld analysis of the neutron diffraction pattern at  $p = 0.63$  Gpa and  $T = 250$  K. Areas with strong contributions from the pressure cell are excluded.

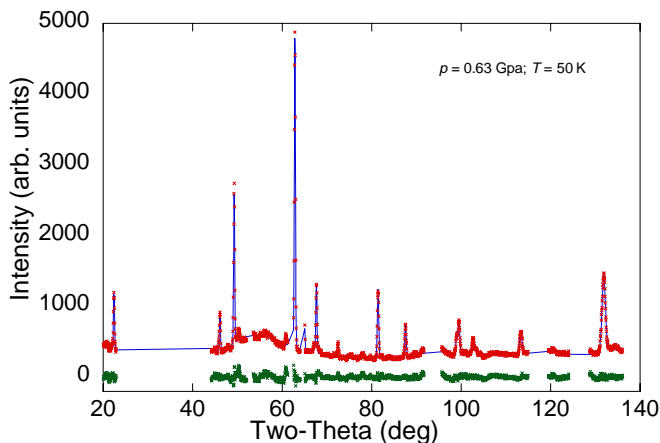


FIG. 5: (color online) Rietveld analysis of the neutron diffraction pattern at  $p = 0.63$  Gpa and  $T = 50$  K. Areas with strong contributions from the pressure cell are excluded.

sequent Rietveld refinements using the GSAS software package. For each diffraction pattern approximately 70 reflections were used to refine the lattice parameters, the  $z$  coordinate of the As ions and the 12 parameters associated with corrections for preferred orientation. We point out that the correction for preferred orientation remained constant over all pressures and temperatures measured and were taken as constants in the fits. Typical  $R$ -values ( $wRp$ ), representing the goodness-of-fit, were between 4-5% for all fits demonstrating the accuracy of the model employed.

## APPENDIX B: DETAILS OF THE SPIN-POLARIZED TOTAL ENERGY CALCULATIONS

For the spin-polarized and non-spin-polarized calculations, the local density approximation was employed, using the full potential linearized augmented plane wave method with the Perdew-Wang 1992 functional. The convergence criterion for the total energy was 0.01 mRyd/cell. The calculations were done in the tetragonal phase (two formula units) for two different cell volumes as the  $c/a$  ratio was varied: 0% volume reduction using the experimentally determined lattice parameters and for a 5% volume reduction. The calculations were also performed for the orthorhombic phase, with  $a/b = 1.02$ , for both 0% and 5% volume reduction. The experimental value of the internal parameter was used for the calculations. The  $R_{MT} * K_{max}$  that determines matrix size (the number of the basis functions), where  $R_{MT}$  is the smallest of all atomic sphere radii and  $K_{max}$  is the plane wave cut-off was set to 8.0. The muffin-tin radii ( $R_{MT}$ ) for the 0% volume reduction calculation were 2.2, 2.1 and 2.1 atomic unit for Ca, Fe and As, respectively. For the 5% reduction calculation, the  $R_{MT}$  also were scaled to keep the matrix size the same. There were 100  $k$  points used in the irreducible Brillouin zone.

- 
- [1] Y. Kamihara, T. Watanabe, M. Hirano, and H. Hosono, *J. Am. Chem. Soc.* **130**, 3296 (2008).
  - [2] H. Takahashi, K. Igawa, K. Arii, Y. Kamihara, M. Hirano, and H. Hosono, *Nature (London)* **453**, 376 (2008).
  - [3] X. H. Chen, T. Wu, G. Wu, R. H. Liu, H. Chen, and D. F. Fang, *Nature (London)* **453**, 761 (2008).
  - [4] M. Rotter, M. Tegel, and D. Johrendt, *Phys. Rev. Lett.* **101**, 107006 (2008).

TABLE I: Results of Rietveld refinements for pressure-dependent measurements at a temperature  $T = 50$  K

Pressure $p$ (GPa)	0	0.115	0.24	0.35	0.47	0.63
$a$ (Å)	5.5312(2)	5.5294(2)	5.5275(2)	3.9792(1)	3.9785(1)	3.9780(1)
$b$ (Å)	5.4576(2)	5.4577(2)	5.4575(2)			
$c$ (Å)	11.683(1)	11.6625(8)	11.6391(9)	10.6379(6)	10.6178(7)	10.6073(7)
Volume $V$ (Å <sup>3</sup> )	352.68(4)	351.94(3)	351.11(3)	168.44(1)	168.07(1)	167.85(1)
$z_{As}$	0.3689(5)	0.3693(4)	0.3690(4)	0.3687(7)	0.3657(7)	0.3663(5)
Fe-As (Å)	2.388(6)	2.3891(3)	2.3854(3)	2.3560(4)	2.343(3)	2.340(3)
Fe-Fe (Å) (2x)	2.7656(1)	2.76469(8)	2.7637(1)			
Fe-Fe (Å) (2x)	2.7288(1)	2.72882(7)	2.72874(8)			
Fe-Fe (Å) (4x)				2.8137(9)	2.8132(1)	2.8128(1)

TABLE II: Results of Rietveld refinements for pressure-dependent measurements at a pressure  $p = 0.63$  GPa

Temperature $T$ (K)	4 ( $p = 0.47$ GPa)	50	100	150	200	250	250 ( $p = 0$ GPa)
$a$ (Å)	3.9797(3)	3.9780(1)	3.9760(3)	3.9724(2)	3.9015(2)	3.8944(2)	3.8915(1)
$c$ (Å)	10.628(1)	10.6073(7)	10.633(1)	10.683(1)	11.438(2)	11.530(2)	11.690(1)
Volume $V$ (Å <sup>3</sup> )	168.33(3)	167.85(1)	167.95(3)	168.57(3)	174.11(3)	174.87(3)	177.04(2)
$z_{As}$	0.365(2)	0.3663(5)	0.3668(9)	0.3669(9)	0.367(1)	0.3652(8)	0.372(1)
Fe-As (Å)	2.333(9)	2.340(3)	2.344(5)	2.346(5)	2.365(9)	2.357(5)	2.410(9)
Fe-Fe (Å) (4x)	2.8141(2)	2.8128(1)	2.8115(2)	2.8089(2)	2.7588(2)	2.7538(1)	2.7517(1)

- [5] C. de la Cruz, Q. Huang, J. W. Lynn, J. Li, W. Ratcliff II, J. L. Zarestky, H. A. Mook, G. F. Chen, J. L. Luo, N. L. Wang, and P. Dai, *Nature (London)* **453**, 899 (2008).
- [6] H.-H. Klauss, H. Luetkens, R. Klingeler, C. Hess, F. J. Litterst, M. Kraken, M. M. Korshunov, I. Eremin, S.-L. Drechsler, R. Khasanov, A. Amato, J. Hamann-Borrero, N. Leps, A. Kondrat, G. Behr, J. Werner, and B. Büchner, *Phys. Rev. Lett.* **101**, 077005 (2008).
- [7] C. Krellner, N. Caroca-Canales, A. Jesche, H. Rosner, A. Ormeci, and C. Geibel, *Phys. Rev. B* **78**, 100504(R) (2008).
- [8] Q. Huang, Y. Qiu, W. Bao, M. A. Green, J. W. Lynn, and Y. C. Gasparovic, T. Wu, G. Wu, X. H. Chen, arXiv:0806.2776 (2008) (unpublished).
- [9] A. Jesche, N. Caroca-Canales, H. Rosner, H. Borrmann, A. Ormeci, D. Kasinathan, K. Kaneko, H. H. Klauss, H. Luetkens, R. Khasanov, A. Amato, A. Hoser, C. Krellner, and C. Geibel, arXiv:0807.0632 (2008) (unpublished).
- [10] A. I. Goldman, D. N. Argyriou, B. Ouladdiaf, T. Chatterji, A. Kreyssig, S. Nandi, N. Ni, S. L. Bud'ko, P. C. Canfield, and R. J. McQueeney, *Phys. Rev. B* **78**, 100506(R) (2008).
- [11] J. Zhao, W. Ratcliff II, J. W. Lynn, G. F. Chen, J. L. Luo, N. L. Wang, J. Hu, and P. Dai, *Phys. Rev. B* **78**, 140504(R) (2008).
- [12] G.-F. Chen, Z. Li, G. Li, W.-Z. Hu, J. Dong, J. Zhou, X.-D. Zhang, P. Zheng, N.-L. Wang, and J.-L. Luo, *Chin. Phys. Lett.* **25**, 3403 (2008).
- [13] K. Sasmal, B. Lv, B. Lorenz, A. M. Guloy, F. Chen, Y.-Y. Xue, and C.-W. Chu, *Phys. Rev. Lett.* **101**, 107007 (2008).
- [14] G. Wu, H. Chen, T. Wu, Y. L. Xie, Y. J. Yan, R. H. Liu, X. F. Wang, J. J. Ying, and X. H. Chen, *J. Phys.: Condens. Matter* **20**, 422201 (2008).
- [15] Z.-A. Ren, G.-C. Che, X.-L. Dong, J. Yang, W. Lu, W. Yi, X.-L. Shen, Z.-C. Li, L.-L. Sun, F. Zhou, and Z.-X. Zhao, *Europhys. Lett.* **83**, 17002 (2008).
- [16] H. Kito, H. Eisaki, and A. Iyo, *J. Phys. Soc. Jpn.* **77**, 063707 (2008).
- [17] M. S. Torikachvili, S. L. Bud'ko, N. Ni, and P. C. Canfield, *Phys. Rev. Lett.* **101**, 057006 (2008).
- [18] N. Ni, S. Nandi, A. Kreyssig, A. I. Goldman, E. D. Mun, S. L. Bud'ko, and P. C. Canfield, *Phys. Rev. B* **78**, 014523 (2008).
- [19] T. Park, E. Park, H. Lee, T. Klimczuk, E. D. Bauer, F. Ronning, and J. D. Thompson, *J. Phys.: Condens. Matter* **20**, 322204 (2008).
- [20] P. L. Alireza, J. Gillett, Y. T. C. Ko, S. E. Sebastian, and G. G. Lonzarich, arXiv:0807.1896 (2008) (unpublished).
- [21] P. C. Canfield and Z. Fisk, *Phil. Mag. B* **65**, 1117 (1992).
- [22] T. Yildirim, arXiv:0807.3936 (2008) (unpublished).
- [23] A. C. Larson and R. B. von Dreele, GSAS (General Structure Analysis System). Los Alamos National Laboratory Report LA-UR-86-748 (1994).
- [24] J. P. Perdew and Y. Wang, *Phys. Rev. B* **45**, 13244 (1992).
- [25] C. H. Lee, A. Iyo, H. Eisaki, H. Kito, M. T. Fernandez-Diaz, T. Ito, K. Kihou, H. Matsuhata, M. Braden, and K. Yamada, *J. Phys. Soc. Jpn.* **77**, 083704 (2008).
- [26] J. Zhao, Q. Huang, C. de la Cruz, S. Li, J. W. Lynn, Y. Chen, M. A. Green, G. F. Chen, G. Li, Z. Li, J. L. Luo, N. L. Wang, and P. Dai, arXiv:0806.2528 (2008) (unpublished).
- [27] Y. Qiu, W. Bao, Q. Huang, T. Yildirim, J. M. Simmons, M. A. Green, J. W. Lynn, Y. C. Gasparovic, J. Li, T. Wu, G. Wu, and X. H. Chen, arXiv:0806.2195 (2008) (unpublished).
- [28] Y. Qiu, M. Kofu, W. Bao, S.-H. Lee, Q. Huang, T. Yildirim, J. R. D. Copley, J. W. Lynn, T. Wu, G. Wu, and X. H. Chen, *Phys. Rev. B* **78**, 052508 (2008).
- [29] J.-W. G. Bos, G. B. S. Penny, J. A. Rodgers, D. A. Sokolov, A. D. Huxleyac, and J. P. Attfield, *Chem.*

- Commun., 3634 (2008).
- [30] J. Dong, H. J. Zhang, G. Xu, Z. Li, G. Li, W. Z. Hu, D. Wu, G. F. Chen, X. Dai, J. L. Luo, Z. Fang, and N. L. Wang, *Europhys. Lett.* **83**, 27006 (2008).
- [31] A. Chubukov, D. Pines, and J. Schmalian, In: K.-H. Bennemann and J. B. Ketterson (eds.), *The Physics of Superconductors*. Springer (2002).